Heliyon 10 (2024) e30844

Contents lists available at ScienceDirect

Heliyon

journal homepage: www.cell.com/heliyon

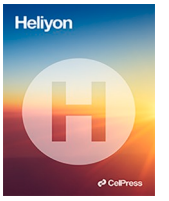

Research article

High-yield fabrication of monodisperse multilayer nanofibrous microparticles for advanced oral drug delivery applications

Fatemeh Ajalloueian [a,b,*], Lasse Højlund Eklund Thamdrup [a,b], Chiara Mazzoni [a,b], Ritika Singh Petersen [c], Stephan Sylvest Keller [c], Anja Boisen [a,b]

[a] Department of Health Technology, Technical University of Denmark, 2800, Kgs. Lyngby, Denmark
[b] The Danish National Research Foundation and Villum Foundation's Center for Intelligent Drug Delivery and Sensing Using Microcontainers and Nanomechanics (IDUN), Department of Health Technology, Technical University of Denmark, Ørsted Plads, 2800, Kgs. Lyngby, Denmark
[c] National Centre for Nano Fabrication and Characterization, DTU Nanolab, Technical University of Denmark, 2800, Kgs. Lyngby, Denmark

ARTICLE INFO

Keywords:
Multilayer nanofibrous microparticles
Sequential electrospinning
Micro-cutting
Oral drug delivery
Tunable release
Compactness

ABSTRACT

Recent advances in the use of nano- and microparticles in drug delivery, cell therapy, and tissue engineering have led to increasing attention towards nanostructured microparticulate formulations for maximum benefit from both nano- and micron sized features. Scalable manufacturing of monodisperse nanostructured microparticles with tunable size, shape, content, and release rate remains a big challenge. Current technology, mainly comprises complex multi-step chemical procedures with limited control over these aspects. Here, we demonstrate a novel technique for high-yield fabrication of monodisperse monolayer and multilayer nanofibrous microparticles (MoNami and MuNaMi respectively). The fabrication procedure includes sequential electrospinning followed by micro-cutting at room temperature and transfer of particles for collection. The big advantage of the introduced technique is the potential to apply several polymer-drug combinations forming multilayer microparticles enjoying extracellular matrix (ECM)-mimicking architecture with tunable release profile. We demonstrate the fabrication and study the factors affecting the final three-dimensional structure. A model drug is encapsulated into a three-layer sheet (PLGA-pullulan-PLGA), and we demonstrate how the release profile changes from burst to sustain by simply cutting particles out of the electrospun sheet. We believe our fabrication method offers a unique and facile platform for realizing advanced microparticles for oral drug delivery applications.

1. Introduction

Oral drug delivery has been recognized as one of the most attractive methods among various delivery routes. Oral dosage forms are still the gold standard for the treatment and management of chronic and debilitating diseases, such as infections, cancer, neurodegenerative and psychotropic disorders [1]. Ease of administration, potential for applying solid formulations providing sustained delivery and long shelf life are key reasons for the significant tendency towards using oral delivery systems. Especially, several pharmaceutical investigations have focused on developing oral dosage forms for tunable sustained drug release [2,3]. Compared to conventional single-unit oral dosage forms (e.g. tablets, capsules, films, or liquids [4]), recently, micro- or nanoparticulate dosage

* Corresponding author.
E-mail address: faaj@dtu.dk (F. Ajalloueian).

https://doi.org/10.1016/j.heliyon.2024.e30844
Received 21 February 2024; Accepted 7 May 2024
Available online 8 May 2024

forms have gained increasing interest for development of novel gastrointestinal drug delivery systems (DDS) [5–7]. The main reason is that a large number of separate subunits of a specific size are administered per each dose of drug. This characteristic alleviates challenges such as unpredictable disintegration, nonspecific drug release, or dose dumping which are associated with use of single-unit forms [8,9]. When comparing micro- and nanoparticles, some superiorities have been reported for nanoparticles. The larger surface-area-to-volume ratio of nanoparticles can provide a larger surface area for interaction with the mucosal surface and for the solubilization of drugs. This results in more uniform drug distribution in the gastrointestinal tract (GIT), elevated drug release, increased residence time of particles in the GIT, as well as higher cellular uptakes [10–13], which altogether leads to increased bioavailability for the loaded drugs especially for poorly soluble hydrophobic ones [14]. There are, however, some drawbacks associated with the use of nanoparticles for oral drug delivery. Premature drug leakage is a major drawback for applications like colon-targeted drug delivery [15]. In parallel, microparticle DDS have demonstrated advantages over nanoparticle systems for applications like peptide or insulin delivery. There, microparticulate formulations can enhance peptide stability, improve protection against enzymatic degradation, and facilitate the handling [16,17]. The above listed characteristics highlight the potential to combine nano- and microparticulate formulations for maximum benefit from both structures. However, it has been a long-lasting challenge realizing nano-structured microparticles for biomedical applications. Independently of the fabrication technology that has been applied, the currently available processes have been unable to provide i) uniform particle size and shape and ii) tuneable multi drug content. The nano-base in these so-called nanostructured microparticles has either been nanoparticles (NPs) or nanofibers (NFs). For NPs, an example is the work by Augustine et al. [14] where they developed a nanoparticle-in-microparticle system for enhanced delivery of hydrophobic drugs in general, along with providing further protection for passage through the stomach. They demonstrated the potential of this structure to treat HIV, where a significantly increased oral bioavailability of antiretrovirals (ARVs) was observed [14]. In such systems, the level of porosity is usually low and there is limited control over distribution of NPs inside the microparticles [18,19]. Regarding NFs, the application of NFs for drug delivery has mostly been limited to electrospun nanofibrous sheets that are used as dressings [20,21]. There have also been a few cases where NFs are used to make microparticulate formulations. In these works, the electrospun NFs have been chopped into individual fibrous segments and further mixed with organic solutions to undergo complex multi-step chemical procedures forming particulate forms [22,23]. Due to several wet-chemical procedures applied post-electrospinning and the risk of premature drug leakage [22,23], these nanostructured microparticles are not appropriate for drug delivery, but have shown promising results for cell-delivery applications [22,23]. Furthermore, the original deeply interconnected web of NFs has been ruined after chopping the NFs. To address this issue, Park and colleagues performed freeze-milling of the original web of nanofibers, followed by suspension and filtration to collect the nanofibrous microparticles. The issue with this method and another study where electrospraying was applied to form nanofibrous microspheres [24,25] is the limited control over the final shape, compactness level and the size of the particles [25].

It is worth noting that electrospinning is the most applied and best suited technique to prepare NFs from a wide selection of materials for diverse biomedical applications [21,26,27], including smart drug delivery [28,29]. Especially, the sequential electrospinning technique allows the users to add various substances or nanomaterials to the electrospinning solution(s) to prepare application-optimized NFs [21,30,31] presenting characteristics such as lightweight, small fiber diameters, inter-connected porosity and high surface-to-volume ratio [20,32–36]. Hence, a simple, fast, and reproducible method to fabricate nanostructured microparticles out of multilayer NFs whilst maintaining the interconnected web inside the microparticles would address the shortcomings of the current technologies. Apart from chemical-based procedures mentioned above, conventional hot embossing or the refined version called hot punching [37] and laser micromachining [38–40] could be considered as options for cutting through NFs and to shape electrospun NFs into micro/nano particles, Whilst the former involves applying high temperatures with the risk of degrading the encapsulated drug or fusion of fibers, the latter would lead to fiber fusion and non-uniform particle formation as tested by us during this study as well. Recently, we proposed micromechanical punching for fabrication of polymeric microparticles out of polymeric films by applying pressure on a Ni stamp at room temperature [41]. In this study, we further developed our technique introducing "micro-cutting" solely relying on pressure-assisted cutting using custom-made ultrasharp silicon tools on multilayer electrospun NFs. The main novelty is successful perforation of single and multi-layer stacks of electrospun fibers to define nanostructured microparticles while preserving the delicate inner structure of the electrospun NFs and protecting the loaded drugs or bioactive agents. A transfer step after cutting also allows for easy harvesting of the microparticles which are residing inside the concave compartments of the micro-cutting tools. In one example of a multilayer construct, we used poly (D, L-lactide-*co*-glycolide) (PLGA) as the external layer and applied pullulan (Pull) as a sandwiched internal layer. PLGA is known as an appropriate hydrophobic biopolymer for fabrication of microparticles due to its ability to 1) protect the encapsulated drug against chemical and enzymatic degradation, 2) enhance oral absorption and 3) control release kinetics [16]. Pull was used as a hydrophilic biopolymer which assists with loading of hydrophilic drugs. We demonstrated the potential to make monodisperse nanofibrous microparticles out of monolayer and multilayer NFs, as well as tunable release profiles for advanced oral drug delivery applications.

2. Materials and methods

2.1. Materials

PLGA with a lactide:glycolide ratio 50:50 and molecular weight of Mw = 54,000–69,000 Da was purchased from Sigma-Aldrich Denmark. Pull (molecular weight ~ 200,000 Da) was kindly donated by Hayashibara Co., Ltd. (Okayama, Japan). Water was purified using a Milli-QPlus 185 water purification system (Millipore, Bedford, MA) with resistivity higher than 18 MΩ cm. Amoxicillin Trihydrate with the purity of >98 % was purchased from TCI chemicals. Dimethyl formamide (DMF), chloroform, and all other

reagents were the analytical grades and purchased from Sigma–Aldrich Denmark. 525 μm thick ⟨100⟩ 4" Si (silicon) substrates were purchased from Topsil GlobalWafers A/S, Frederikssund, Denmark.

2.2. Electrospinning of nanofibrous polymer sheets

To fabricate mono-layer electrospun sheets of Pull or PLGA, the relevant solutions were electrospun onto a stainless steel static collector using a home-made electrospinning setup. For both Pull and PLGA, polymer solutions were loaded into 1 mL syringes fitted with a 21-gauge blunt-end needle, and the electrospinning parameters were set at an applied voltage of 12–14 kV, a collection distance (grounded collector from needle tip) of 15 cm, and an electrospinning solution flow rate of 1.0 mL/h. Electrospinning was performed at room temperature (25 °C) and at a relative humidity of 35 %. For electrospinning of PLGA, PLGA was dissolved in mixed solvent of chloroform/DMF [20] (90:10 v/v) with a concentration of 20 % (w/v). For Pull electrospinning, Pull was dissolved in water with concentration of 20 % w/v as described earlier [42]. To fabricate a multilayer sheet, a three-layer sheet of PLGA-Pull-PLGA was electrospun using the same setup as mentioned above. First, 0.25 mL of PLGA was electrospun using a solution of 20 % PLGA in mixed solvent of chloroform/DMF (90:10 v/v), then a layer of Pull 20 % was added (1 mL), and finally the last layer of PLGA was electrospun on top of the two other layers (0.25 mL). Whilst maintaining the volume ratio of Pull to PLGA as 4:1 per each electrospinning layer, different volumes of PLGA and Pull were used to manage different final thicknesses of 60, 80 and 150 μm in multilayer electrospun sheets.

2.3. Design and fabrication of ultra-sharp micro-cutters

The micro-cutting tools were produced by conventional top-down processing of single-side polished, Si substrates. We fabricated two types of micro-cutters as cylindrical and pyramidal frustums. Initially, to produce cylindrical tools (Fig. 1 (a) – (e)), the Si substrate was subject to wet thermal oxidation (Tempress horizontal furnace, Vaassen, Netherlands) for growing a 1.1 μm thick SiO_2 layer. The resulting oxide layer was masked using conventional UV lithography (MLA100 Tabletop Maskless Aligner, Heidelberg Instruments, Heidelberg, Germany) in 1.5 μm thick positive resist AZ®5214E (MicroChemicals GmbH, Ulm, Germany). The resist was exposed with a dose of 90 mJ/cm^2 @365 nm and developed in AZ® 726 MIF (MicroChemicals GmbH, Ulm, Germany) for 90 s using a single-puddle

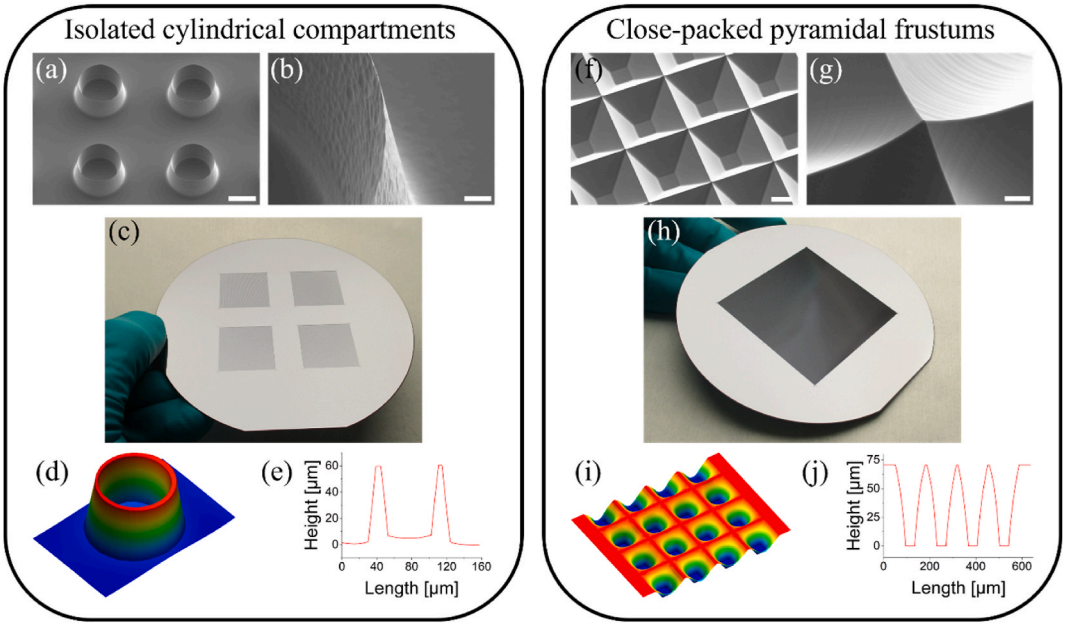

Fig. 1. Pictures, SEM images and topography data pertaining to the two different microfabricated tools. (a) SEM image showing the isolated cylindrical micro-cutters after the final isotropic dry etch. The scale bar corresponds to 40 μm. (b) SEM image acquired at high magnification showing the immensely sharp cutting edge associated with the top part of the tapered sidewalls. The scale bar corresponds to 3 μm. (c) Picture of the final silicon substrate which has four square 20 × 20 mm^2 areas that can be used as tools for micro-cutting. (d) and (e) respectively show 3D topography image and cross-sectional profile based on the VSI data collected prior to the final isotropic dry etch. (f) SEM image showing the close-packed inverse pyramidal frustum micro-cutters after the final isotropic dry etch. The scale bar corresponds to 40 μm. (g) High magnification SEM image showing the smooth surface of the concave compartments and the sharp cutting edge at the top apex of the interconnected sidewalls. The scale bar corresponds to 2 μm. (h) Picture of the final silicon substrate which has a patterned 50 × 50 mm^2 area that can be used for micro-cutting. (i) and (j) 3D topography image and cross-sectional profile based on the VSI data collected prior to the final isotropic dry etch. The measured compartment base length, depth and sidewall taper angle was 130 μm, 70 μm and 53.7°, respectively. (For interpretation of the references to colour in this figure legend, the reader is referred to the Web version of this article.)

approach (Süss MicroTec Gamma 2 M developer, Garchen, Germany). The resulting resist pattern was transferred to the SiO_2 layer using an Advanced Oxide Etcher (AOE, STS MESC Multiplex ICP) with 5 sccm C_4F_8, 4 sccm H_2 and 174 sccm He as the reactive gasses. The chamber pressure during etch was 4 mTorr, the coil|platen power was adjusted to 1300 W|200 W and the platen temperature was 0 °C. This effectively results in an oxide hard mask that can be used for etching deep into the Si substrate. Prior to the Si etching steps, the resist was stripped using a combination of energetic oxygen plasma in a barrel asher (300 Semi Auto Plasma Processor, PVA TePla America Inc.) and submersion into 7-up at 80 °C. The 7-up consists of concentrated H_2SO_4 with $(NH_4)_2S_2O_8$ salt added just prior to immersion into the solution that effectively strips any remaining traces of resist. The first step in the silicon etching process is a taper etch performed in an Advanced Silicon Etcher (ASE, STS MESC Multiplex ICP). The etch, that creates a slightly tapered (final taper angle = 82°) sidewall profile, uses 75 sccm SF_6 and 60 sccm O_2 with a trace amount of C_4F_8 (5 sccm) added for etching into the silicon. The taper etch was conducted in continuous mode with a platen temperature of 20 °C which resulted in a modest mask undercut and a relatively low surface roughness on the tapered sidewalls. The chamber pressure during etch was 40 mTorr and the coil|platen power was set to 2000 W|15 W. The cylindrical protrusions, constituting the sidewalls, were etched to a depth of approximately 55 μm and the remaining SiO_2 mask was stripped in buffered hydrofluoric acid (12 vol% HF with NH_4F). Prior to the oxide removal, the wafer was cleaned using oxygen plasma and a mixture of concentrated H_2SO_4 and H_2O_2 (i.e., Piranha, H_2SO_4:H_2O_2 = 4:1). The tapered sidewalls were subsequently subject to a dry isotropic etch in the ASE which was performed to reduce surface roughness and ultimately to increase the sharpness of the cutting edges. The isotropic etch was merely implemented by omitting the passivation step in the Bosch process which is used for silicon deep etch. The reactive gasses were 230 sccm SF_6 and 23 sccm O_2 and the substrate temperature was kept at 20 °C. A manual pressure setting of 87.7 % was used and the coil|platen power was fixed at 2800 W|19 W.

To increase the mechanical robustness of the microfabricated tools and simultaneously increase the number of particles produced per cutting cycle, a new design was devised and the pyramidal frustum Si tools were fabricated using a combination of wet anisotropic etching using a SiO_2 hard mask and dry isotropic etching (Fig. 1 (f)–(j)). Initially, a 1.1 μm thick SiO_2 layer was grown on a silicon substrate using wet thermal oxidation. The oxide layer was masked using UV lithography (MLA150 WM I, Maskless Aligner, Heidelberg Instruments, Heidelberg, Germany) in 1.5 μm thick positive resist AZ®5214E. In the UV lithography step, automatic flat alignment was employed, and the resist was exposed using a dose of 75 mJ/cm^2 @375 nm before developing the exposed resist for 90 s in AZ® 726 MIF using a single-puddle approach. The underlying SiO_2 layer was then subject to an AOE dry etch followed by oxygen plasma and 7-up to remove traces of resist and contaminants (refer to details above). To achieve moderately tapered sidewalls, wet anisotropic etching of silicon was used. The SiO_2 masked substrate was immersed in 28 wt% KOH heated to 80 °C to ramp up the silicon etching rate. As the anisotropic KOH etch features major differences in the etch rates along different crystal orientations, concave compartments having an inverse pyramidal frustum shape were produced in the unmasked portions of the silicon substrate. As described above, the remaining SiO_2 hard mask was stripped in buffered hydrofluoric acid and the substrate was immersed in 7-up heated to 80 °C to clean the surface prior to the final isotropic dry etch. In order to sculpt the top portion of the interconnected sidewalls for provision of sharp cutting edges, a brief isotropic dry etch was carried out on the ASE (refer to details above). This step

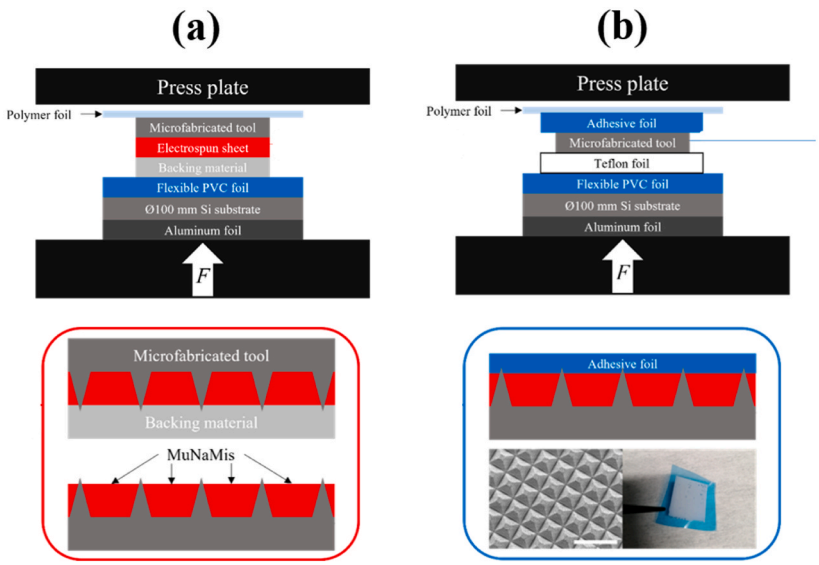

Fig. 2. Schematics illustrating the micro-cutting process (a) and the subsequent transfer step (b). As shown, two similar stacks are used for micro-cutting and transfer. The aluminum foil, silicon substrate and the flexible PVC foil are used to protect the lower press plate and to ensure a planar surface during micro-cutting. The polymer foil used on the top of the stacks is to protect both the upper press plate as well as the microfabricated tool. The Teflon foil used during release of the MuNaMi is partly to prevent stiction of the mildly adhesive foil to the flexible PVC foil on the silicon substrate. The inserts in the bottom row on the left side show a SEM image of pyramidal frustum MuNaMi after release (scale bar corresponds to 200 μm) and a picture of the adhesive foil after transfer of close-packed pyramidal frustum MuNaMi. (For interpretation of the references to colour in this figure legend, the reader is referred to the Web version of this article.)

effectively results in sidewall tip apex widths in the sub-1 μm regime which is needed for efficiently cutting through the electrospun sheets. To alleviate potential stiction of the micro-cut particles, the silicon tools were cleaned using oxygen plasma prior to immersion in piranha solution and deposition of an anti-stiction coating. This coating was deposited using molecular vapor deposition (MVD 100 Molecular Vapor Deposition System, Applied Microstructures Inc., San Jose, CA, USA) where a self-assembled conformal monolayer of 1H,1H,2H,2H-perflourodecyltrichlorosilane (FDTS) is formed on the exposed silicon surface. In a final step, the FDTS-coated silicon substrates were diced out into suitable square formats (20 × 20 mm^2 or 25 × 25 mm^2) using a conventional wafer dicing saw (Automatic Dicing Saw DAD 321, Disco Corporation, Tokyo, Japan) equipped with a diamond blade.

2.4. Micro-cutting process

For production of MuNaMi, an industrial hot embosser (Collin Press P300 SV, Collin Lab & Pilot Solutions GmbH, Maitenbeth, Germany) was used. The hot embosser delivers a planar parallel pressure in the range from 1.5 to 250 bar on a working area of 295 × 295 mm^2. The micro-cutting process can be divided into two steps, as schematically shown in Fig. 2, each with a cycle time of approximately 30 s: i) the actual cutting, where the sharp edges of the microfabricated tool penetrates through the ES and slightly into the backing material to produce discrete monodisperse microparticles (Fig. 2a) and ii) the transfer of the produced microparticles (Fig. 2b) from the microfabricated tool onto a 65 μm thick plasticized polyvinylchloride (PVC) foil with a 10 μm thick layer of pressure sensitive acrylic-based adhesive (Nitto Semiconductor Wafer Tape SWT 20+R, Nitto Denko Corporation, Osaka, Japan). Two similar stacks are used during cutting and transfer. To protect the lower press plate while simultaneously ensuring a planar and non-rough surface during cut and release, the stacks comprise a 50 μm thick aluminum foil and a ø100 mm single-side polished silicon substrate onto which a flexible PVC foil has been attached (same foil as used during release). As backing material, a high quality aluminum foil (Al foils for thermal imprinting, Obducat Technologies AB, Lund Sweden) with a thickness of approximately 75 μm was used. The Al foil ensures a minimal degree of strain in a plane perpendicular to the applied force during micro-cutting. This is beneficial in terms of minimizing potential deformation of the produced MuNaMi. During the transfer cycle, the backing material was substituted with a 150 μm thick Teflon sheet (Polyfluor Plastics, Minervum, Netherlands) which serves as a flexible anti-stick cushion. The adhesive foil is merely placed on the microstructured surface of the tool and covered by an approximately 100 μm thick polypropylene foil which serves as a protective cushion between the upper press plate and the microfabricated tool.

2.5. Surface free energy measurement

The surface free energy measurement on the FDTS coated reference sample was carried out by drop shape analysis (DSA30, KRÜSS GmbH, Hamburg, Germany). Based on contact angle measurements on droplets of deionized water (2 μl) and diiodomethane (1 μl) the surface free energy was evaluated using the Owens, Wendt, Rabel and Kaelble (OWRK) method.

2.6. Drug-loading into nanofibers

Amoxicillin (AMX) was used as a model drug in this study. AMX was loaded into Pull NFs with a concentration of 5 % w/w (weight of AMX to the weight of polymer), where AMX:Pull is the sandwiched internal layer forming a three-layer construct as mentioned above. Similar to our previous work [20], for encapsulation of AMX in Pull, AMX was dissolved in water and then Pull was added to the solution to reach the desired concentration. The 5 % AMX-Pull solution was prepared using a 1 % aqueous suspension of AMX. For fabrication of drug-loaded MuNaMi constructs, cutting over PLGA-AMX:Pull-PLGA multilayer sheets was performed using a close-packed pyramidal frustum micro-cutter. The loading dose of AMX in the final particles is therefore 5 % of the Pull relevant mass or 3.33 % of the total mass of the MuNaMi.

2.7. In vitro release of AMX

The amount of AMX loaded into the MuNaMi and the release kinetics were assessed. Around 2 mg MuNaMi with or without AMX were loaded into gelatin capsules (Torpac size 9; Fig. 1s). The capsules were coated in a 12 % (w/v) solution of Eudragit L100 in IPA where dibutyl sebacate was added as plasticizer in a 5 % w/w ratio relative to Eudragit. At the beginning of the experiment, one capsule was inserted in a cellulose membrane dialysis tubing (MW cut off 12,000 Da), the ends were sealed, and it was placed in a beaker containing 5 mL of 0.02 M HCl solution with pH 1.7 simulating the acidic conditions present in the stomach. 200 μL samples were taken after 5, 15, 30 and 60 min and the corresponding volume was replaced each time with fresh 0.02 M HCl solution. Next, the dialysis bags were transferred into 5 mL phosphate buffer with pH 7.5 simulating the transition to the intestinal environment. 200 μL samples were taken after 5, 10, 20, 30, 45, 60, 90, 120, 240, 360 min and 24 h and the corresponding volume was replaced each time with fresh phosphate buffer. All the samples were frozen at −18 °C and stored for HPLC analysis.

2.8. High pressure liquid Chromatography (HPLC) analysis

The samples from the drug release test from PLGA-AMX:Pull-PLGA MuNaMi were analyzed using HPLC. The release data was compared with the results of AMX release from AMX:Pull monolayer and PLGA-AMX:Pull-PLGA multilayer sheet investigated in our previous work [20]. Analysis was performed using a reverse-phase C18 column HPLC. Prior to analysis, samples were thawed at room temperature and well mixed. AMX was analyzed as previously described by Christfort et al. [43] Briefly, the HPLC was run in isocratic

mode and mobile phases were constituted of : A) 6.8 g/L of potassium phosphate monobasic in deionized water and B) deionized water with 5 % v/v acetonitrile. The ratio of the mobile phases A:B was 95:5 v/v. Samples were run using a Luna 5 μm C18 100 Å, 250 × 4.6 mm column (Phenomenex ApS, Nordic Region, Værløse, Denmark) at room temperature. The injected volume was 20 μL with a flow rate of 1 mL/min and a total run time per sample of 10 min. The wavelength selected for measuring absorbance was 230 nm. Two calibration curves were prepared using a 0.5 mg/mL amoxicillin stock solution dissolved in either 0.02 HCl solution or in phosphate buffer. The calibration range chosen was between 0.1 μg/mL and 100 μg/mL.

2.9. FTIR analysis of electrospun constructs

Characteristic absorption bands of the electrospun pure nanofibers (Pull and PLGA), powder of AMX, AMX-loaded Pull, and the layered construct of PLGA-AMX:Pull were determined by Fourier-transform infrared spectroscopy (FTIR). A PerkinElmer Spectrum 100 spectrometer (Waltham, Massachusetts, USA), based on a Universal Attenuated Total Reflectance sensor 125 (UATR-FTIR) was applied to record the FTIR spectra in the transmission mode over a range of 4000–650 cm^{-1}. Automatic signals were recorded in 4 scans, and the spectra were plotted as a function of wavenumber (cm^{-1}).

2.10. Topography and morphological characterization

The topographies of the microfabricated tools were characterized using a combination of optical microscopy (Nikon ECLIPSE L200, Tokyo, Japan), vertical scanning interferometry (PLu Neox 3D Optical Profiler, Sensofar Metrology, Terrassa, Spain) and scanning electron microscopy (SEM, Zeiss Supra 40 VP, Jena, Germany). The morphology of electrospun sheets forming different MuNaMi constructs were also analyzed using SEM. Samples were mounted on stubs and were coated with a thin layer of platinum to increase conductivity for SEM imaging.

3. Results and discussion

3.1. Custom-made micro-cutters

The overall aim of this proof-of-concept study was to develop a robust and functional method for cutting microparticles out of electrospun nanofibrous sheets and ultimately demonstrate the potential use of these particles for oral drug delivery applications. To the best of our knowledge, there are no previous reports on an efficient and reproducible method for high yield production of such particles. In order to achieve this goal, initial experiments were conducted applying laser ablation on electrospun constructs, similar to other works [44,45]. According to investigations, laser ablation can be considered as an effective method to pattern ES with various thicknesses of 60–120 μm. However, it was not feasible to obtain microparticles with uniform size and complete cutting using the laser ablation technique with the available tools. To achieve a more robust and reproducible technique, we considered to apply custom-made Si tools to cut through drug-loaded ES. Taking into account the sensitivity of some drugs/bioactive agents to high temperature, the aim was to avoid the use of high temperature in this process. Instead, pressure alone was applied as the driving force during micro-cutting.

To produce substantial amounts of monodisperse MuNaMi by micro-cutting at room temperature, suitable tools were fabricated as shown in Fig. 1. The tools feature a designed topography consisting of near vertical or tapered sidewalls having ultrasharp cutting edges with a width (or conversely, radius of curvature) substantially below 1 μm. Essentially, micro-cutting bears resemblance to conventional mechanical punching in which a matching die and punch set is used for producing e.g. metal or rubber components in an industrial setting. As presented here, the term micro-cutting is used to describe a process in which the microfabricated tool is pressed into an ES comprising one or more layers. In the process, which is carried out at room temperature, no counter die is needed. Instead, a backing material is used. The hardness of the backing material must preferably exceed the hardness of the ES. Conversely, the hardness should be lower than the hardness associated with the cutting edges of the microfabricated tools. The reduced taper angle associated with the close-packed compartments causes a continuous increase in the effective contact area between the tool and the sheet which increases the through-cut force significantly. It is essential to ensure that the cutting edges have penetrated the full thickness of the ES before terminating the cutting cycle. This was verified by microscopy inspection of the microfabricated tool prior to initiating the release of particles from the micro-cutting tool. Likewise, during the transfer phase (Fig. 2b), the applied force must be sufficient for establishing a conformal contact between the adhesive foil and the backside of the MuNaMi. In general, a force of approximately 500 N/cm^2 was applied for 30 s during transfer. Due to the nanofibrous morphology of the produced MuNaMi and the intrinsically low surface free energy and surface roughness of the FDTS coated tool, no microparticle adhesion to the microfabricated tool was observed. The surface free energy of FDTS coated silicon was determined by drop shape analysis on a planar reference sample to be 7.5 mJ/m^2, ensuring that MuNaMi can easily detach from the concave silicon compartments after the mechanical micro-cutting process. After the transfer cycle, the microparticles could easily be collected from the adhesive foil using a razor blade or a scalpel. It is worth noting that the frustum pyramid cutting tools were reusable for numerous cutting cycles. For more durability, new micro-cutting tools in other materials such as metals and/or alloys are being made.

3.2. Fabrication of hemispherical MuNaMi

The cylindrical micro-cutter was applied for fabrication of hemi-spherical microparticles. The isolated cylindrical compartments

were arranged in a 2D array with a period of 150 μm in both directions. The inner diameter associated with the cutting edge at the top of the sidewalls was approximately 70 μm and the sidewall taper angle was found to be 82° based on the VSI data. The inner depth, or conversely the sidewall height, of the cylindrical compartments was found to be 55 μm and the surface roughness of the sidewalls was kept minimal to impede MuNaMi adhesion related to potential mechanical interlocking after micro-cutting. The cutting edge width was estimated from SEM images and it was found to be approximately 100 nm which, in combination with the relatively high sidewall taper angle, ensured a clean cut through the ES. The tools featuring the isolated cylindrical micro-cutters were 20 × 20 mm^2 which allowed for simultaneous production of 17689 microparticles in a single cutting cycle. In the micro-cutting step, the sharp cutting edges of the microfabricated tool promote a localized deformation of the nanofibrous sheet. Cutting occurs when the ultimate fracture strain is reached, which happens across sharp cutting edges. The required cutting force depends intimately on the ES thickness and composition as well as the topography of the microfabricated tool. In the current study, the thickness of the ES was similar to or slightly larger than the concave compartment depth in the tools. In general, a micro-cutting force of approximately 1000 N/cm^2 or 3600 N/cm^2 was needed to obtain through-cuts using the isolated cylindrical compartment tool or the close-packed pyramidal frustum tools respectively. Fig. 3 shows the procedure of using a cylindrical micro-cutter (Fig. 3a) to cut through a mono-layer of electrospun PLGA (thickness of 60 μm; Fig. 3b) and the resulting hemi-spherical microparticles. As illustrated in Fig. 3c, MoNaMi are produced leaving behind a thin perforated ES with a dense 2D array of holes (Fig. 3d). We further tested the feasibility of cutting through different electrospun layers such as pullulan, silk fibroin and chitosan-PEO monolayers. All resulted in around 100 % yield and full-thickness cut-out of the nanofibrous microparticles.

With increasing attention towards the use of multilayer nanofibers for potential loading and delivery of different drugs/bioactive agents [21,27,46,47], we fabricated a three-layer sheet of PLGA-pullulan-PLGA (thickness of 80 μm) and used the ultra-sharp Si cutter to cut through it. As presented in Fig. 4, MuNaMi with same size and shapes were formed using the cutting procedure. The integration of different layers using a combination of selected hydrophilic and/or hydrophobic polymers is an advantage to provide the possibility of loading various types of drugs depending on their solubility, bioavailability and the expected release profile [48,49]. Layered constructs are gaining more and more attention for tuning the drug release depending on the solubility and thickness of the internal sandwiched layer. For instance, Milosevic et al. applied a computational model to validate a prolonged drug release from a three--layered fibrous scaffold (PCL/PLGA/PCL) compared with a monolayer PLGA scaffold. They demonstrated that the three-layer scaffold delays the drug release process, and can be used in postoperative therapy for the time-controlled release of drugs [47]. In this study we investigated PLGA and pullulan to achieve a combination of hydrophobic-hydrophilic biopolymers in the layered construct. PLGA is widely applied in therapeutic formulations due to its biocompatibility and biodegradability, as well as the potential for tailoring a sustained release of encapsulated hydrophobic drugs. On the other side, the hydrophilic pullulan is an edible polymer which is ideal for encapsulating hydrophilic drugs or bioactive agents with poor stability. As shown in Fig. 4, we performed a layer-by-layer sequential electrospinning of PLGA, pullulan and PLGA, respectively, to fabricate three-layer sheet consisting of PLGA-Pullulan-PLGA (Fig. 4a) with approximate thickness of 10 μm, 60 μm and 10 μm for the different layers. The average diameter was 785 ± 423 nm and 282 ± 76 nm for PLGA and pullulan nanofibers, respectively. Pressing the ultra-sharp Si tool into the layered sheet (Fig. 4 (b)) formed MuNaMi (Fig. 4c), where the nanofibers of the top external layer (PLGA fibers shown by arrows in Fig. 4d) extended over the internal layer (pullulan nanofibers shown by circles in Fig. 4d) and covered the whole internal layer.

3.3. Fabrication of pyramidal frustum MuNaMi

The cylindrical cutting tools applied for fabricating semi-spherical particles represent high yield for the expected particles. However, to avoid having excess material after micro-cutting while simultaneously increasing the structural robustness of the microfabricated silicon tools, close-packed inverse pyramidal frustums were used (Fig. 1f). In other words, using this cutter, the entire ES is cut into particles with no excess material. The design features a regular tessellated array of concave compartments where the distance between cutting edges was 135 μm. Based on VSI measurements the sidewall taper angle and compartment depth were found

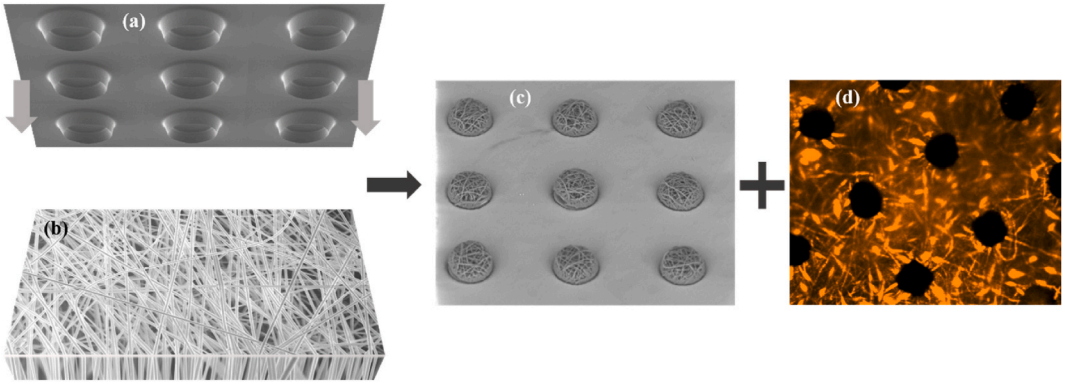

Fig. 3. Representation of applying a cylindrical micro-cutter (a) through a monolayer electrospun PLGA sheet (b), to fabricate hemispherical monolayer nanofibrous microparticles (c) and leaving behind a thin perforated sheet (d).

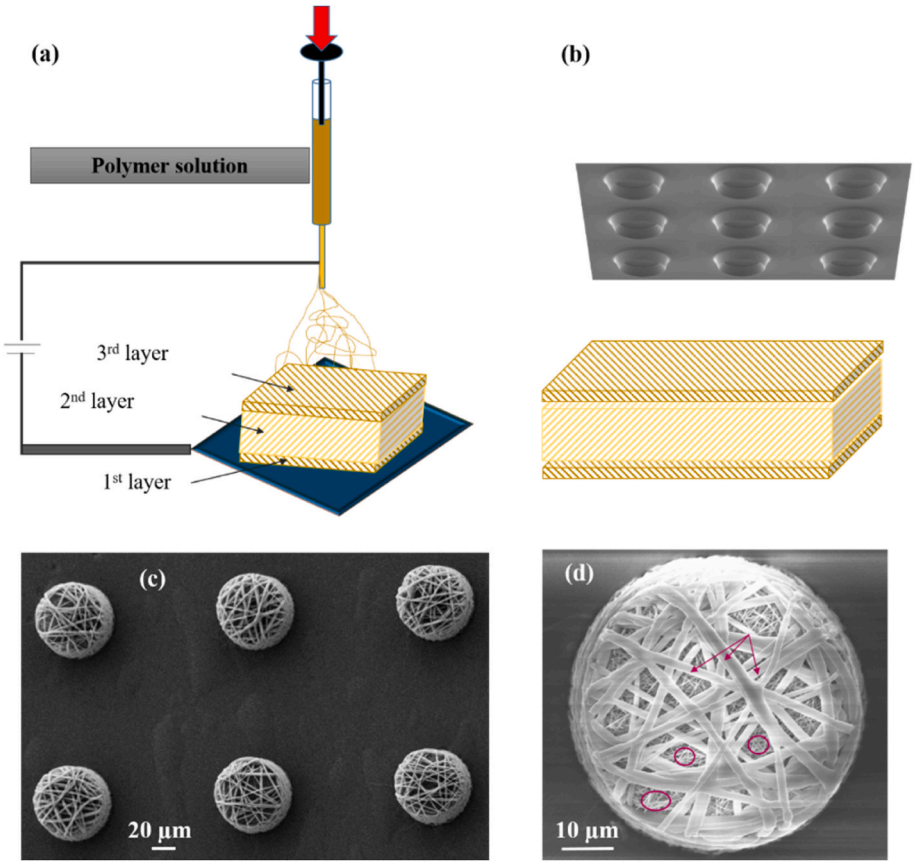

Fig. 4. Schematic representation of the multilayer ES fabricated using sequential electrospinning (a), the procedure of cutting through the multilayer ES using sharp cylindrical micro-cutters (b), the hemispherical MuNaMi cut out of the electrospun layer (c), and the magnified top view representation of the MuNaMi showing the external fibers (PLGA nanofibers shown by arrows) and the internal thinner fibers (pullulan nanofibers shown inside circles).

to be 53.7° and 70 µm, respectively. Due to the fact that the compartments were mainly formed during the anisotropic KOH wet etch, the sidewall surfaces were perfectly smooth and the interconnected cutting edges exhibited widths in the sub-100 nm regime. The tool for fabricating pyramidal frustum MuNaMi was 25 × 25 mm^2 which allowed for producing 33856 microparticles per cutting cycle. As illustrated in Fig. 5, well-oriented rows of MuNaMi were formed (Fig. 5 (a)) by applying the pyramidal frustum micro-cutter (Fig. 5b) onto a multilayer electrospun PLGA-Pullulan-PLGA sheet with approximate thicknesses of 15 µm, 120 µm and 15 µm for the different layers respectively. Applying the close-packed tools led to 100 % yield of MuNaMi (Fig. 5c) which could easily be collected (Fig. 5 (d)). We also performed FTIR analysis to confirm the presence of AMX into Pull fibers, and represent a typical FTIR spectra of the layered construct containing all PLGA, Pull and AMX. According to Fig. 6, among typical absorption bands of AMX at 1686 cm^{-1} and 1519 cm^{-1} (assigned to the amide I and amide II) [50], and other peaks at 1618 cm^{-1}, 1775 cm^{-1} and 3448 cm^{-1} (attributed to benzene ring, the vibration of carboxyl group, and the stretching vibration of amino and hydroxyl group in the AMX structure [51,52]), the AMX peak at 1519 cm^{-1} (shown inside the blue box) could represent the existence of AMX in Pull fibers, demonstrating a weak van der Waals interaction between Pull and AMX without formation of any new bonds. It was difficult to see other AMX signals, probably because some vibration bands of AMX overlapping with those of Pull. It was also shown that in the layered construct making the MuNaMi, the representing peaks of Pull (grey box), PLGA (orange box) and AMX are demonstrated confirming the chemical presence of all three components.

3.4. Drug release from pyramidal frustum MuNaMi

Having optimized the cutting procedure, the next step was to introduce a model drug in the MuNaMi and to study the drug release profile. To investigate how forming nanofibrous electrospun sheets to novel MuNaMi structures affected the drug release, we compared our previous data of AMX release (under pH 7.5) from a monolayer sheet (AMX:Pull) and also a previous data of AMX release (under pH 7.5) from multilayer sheet (PLGA-AMX:Pull-PLGA) [20]) with the *in vitro* release data of the particulate form (MuNaMi). For the MuNaMi study, the particles were placed in enterically coated capsules and the release was measured under two pHs of 1.7 and 7.5. As shown in Fig. 7, there was a burst release from the monolayer sheet of AMX:Pull reaching 100 % in less than 10 min (Fig. 7a), and a

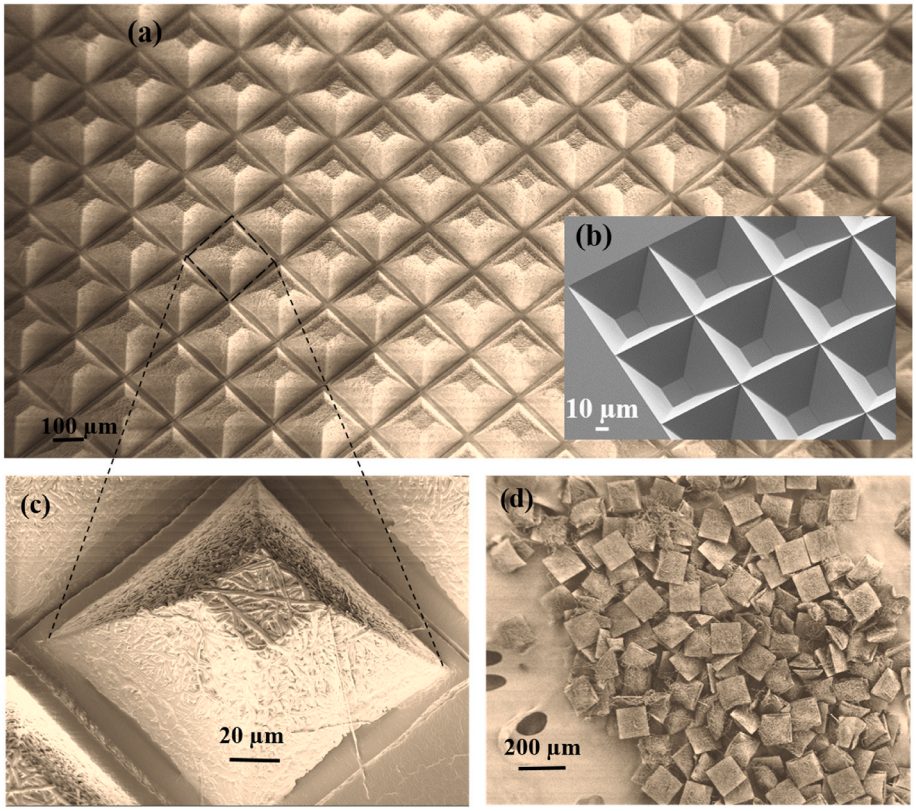

Fig. 5. Pyramidal frustum-shaped microparticles (a) are produced by micro-cutting through a multilayer ES using an ultra-sharp cutting tool (b). An individual fully cut MuNaMi (c) and the collection of particles (d) are also demonstrated.

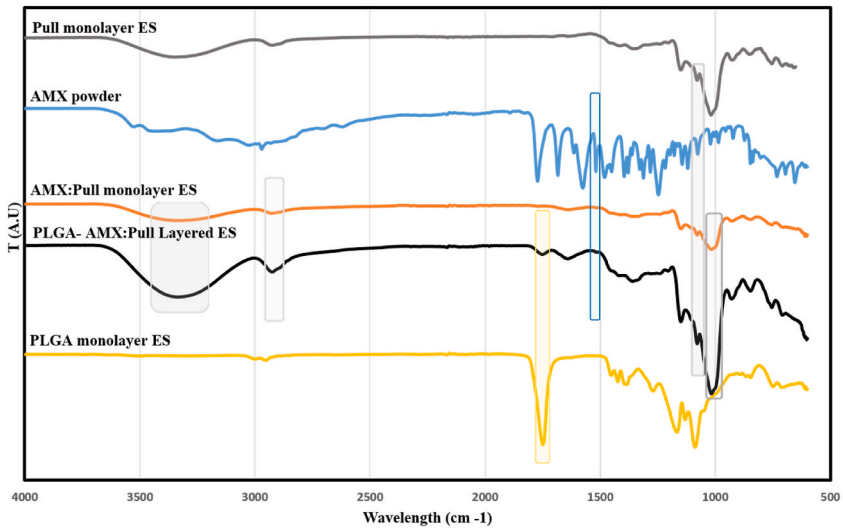

Fig. 6. FT-IR spectra of pure Pull ES, AMX powder, AMX:Pull monolayer ES, layered ES of PLGA-AMX:Pull and pure PLGA ES.

relatively fast release from the multilayer sheet (80 min; Fig. 7 (b)). In comparison, as shown in Fig. 7c, there was no release of AMX from the MuNaMi under acidic conditions (stomach-like environment) during the first hour (thanks to the enteric coating in this step), but a sustained release was observed in pH 7.5 simulating the transition to the intestinal environment. The average release after 7 h in pH 7.5 was around 33 %, and reached around 35 % after 24 h, representing the sustained release of AMX getting dissolved from the hydrophilic fast-dissolving Pull NFs and passing through the PLGA barrier. The sustained release is usually the preferred form of

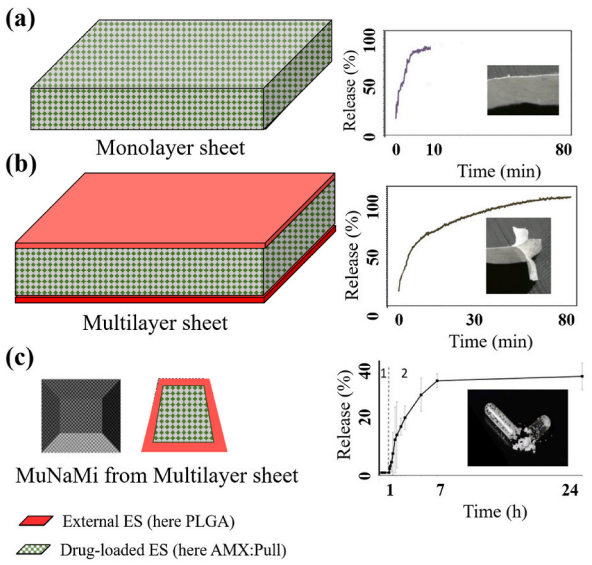

Fig. 7. Representing the role of performing micro-cutting on tuning the release of the model drug (AMX) from different constructs listed as AMX: Pullulan monolayer sheet (a), PLGA-AMX:Pull-PLGA multilayer sheet (b), and the MuNaMi cut out of the PLGA-AMX:Pull-PLGA multilayer sheet (c).

release in drug delivery applications. The drug release profile shown in Fig. 7c could be high enough to give a rapid onset of the desired therapeutic response. Then the trend maintains a constant level for the desired duration of time. The huge difference between releases of AMX from the multilayer constructs in the forms of sheets or particles could be explained by the morphological changes which are given during cutting procedure (further discussed below) leading to different types of mass transport processes [53]. In the monolayer construct, the burst release seems to be related to the dissolution of the fast-dissolving polymeric matrix (Pull), followed by dissolution of the loaded drug (AMX). In the case of the multilayer sheet, the coverage of the hydrophobic PLGA ES seemingly postpones the very burst release. However, the diffusion of water into the system from open margins leads to the dissolution of the Pull layer and release of the loaded AMX, where a rather fast release is observed [36,47]. The case of the MuNaMi is however different. In this specific case, the cutting procedure leads to formation of a core-shell-like structure where the two external PLGA sheet meet each other and play the role of an extra barrier for both diffusion of water into the system, and subsequently the drug diffusion out of the particles through the web of porous PLGA NFs. Although a faster release is observed during the first 7 h, the release is more sustained afterwards. This could be due to the deposition of the dissolved Pull over the PLGA fibers during the out-diffusion, where an extra burden is introduced towards the AMX drug. We believe that the bulk degradation of the PLGA fibers would lead to increased release of AMX during time. Also, decreasing the thickness of the PLGA NFs sandwiching the internal drug-loaded layer could assist with a faster release of the drug, if required. Apparently, in MuNaMi constructs, we face different phases, where defining the slower process per each phase can be considered as the rate-limiting step, to define the overall release model [53]. More in-depth study on the drug(s) release from MuNaMi

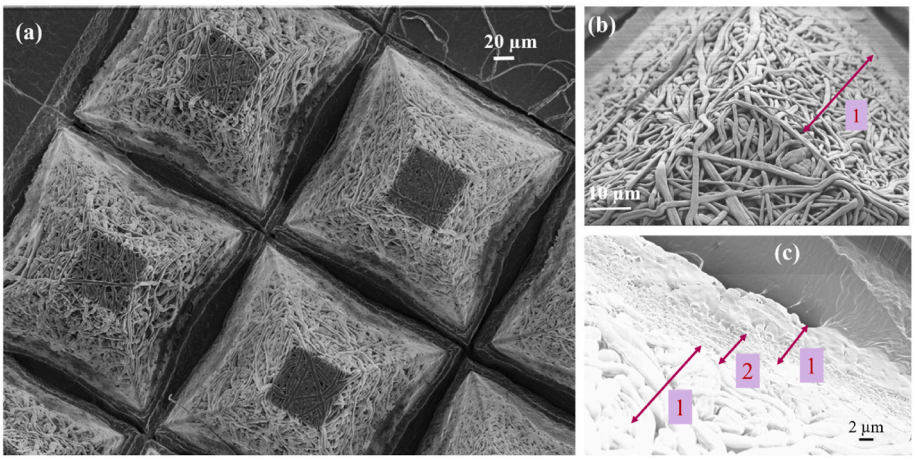

Fig. 8. The overall appearance of frustum pyramid-shaped PLGA-AMX:Pull-PLGA MuNaMi (a) with a close-up view of the exterior part (b) and internal cross-section (c). The exterior part consists completely of thicker PLGA fibers (1 represents PLGA), whilst the internal part consists of three layers of fibers including PLGA (1), Pull (2 represents Pull with finer fibers) and another PLGA (1).

constructs is under consideration in our next studies.

3.5. Three-dimensional structures and compactness of MuNaMi

We observed that cutting through multilayer sheets of PLGA-Pull-PLGA leads to extension of the external layer (here PLGA) where the internal layer is covered partially (Fig. 5d; the internal layer is visible) or fully (Fig. 7c). Especially due to different diameters of PLGA and Pull nanofibers, it was obvious that cutting through the multilayer PLGA-Pull-PLGA with total thickness of 150 μm would lead to a homogenous 3D construct fully covered by PLGA nanofibers (Fig. 8a). In order to better investigate the coverage introduced by extension of the surrounding PLGA layer around the Pull layer, we compared the external and internal structures of the MuNaMi. As illustrated in Fig. 8 (a,b), the external part of the MuNaMi shows the PLGA fibers only, whilst the internal layer (Pull) which is sandwiched between the external layers is visible only in the internal view (Fig. 8c). In other words, it is the extension of the outer layer of PLGA around Pull layer that delays the dissolution of the Pull and hinders the diffusion of the dissolution products from the multilayer particles. This sandwiching of the fast-dissolving Pull layer can explain the sustained release of the AMX from the MuNaMi. The other explanation that can be considered for the transition from fast to sustained release after cutting the multilayer ES sheet to MuNaMi is the effect of compression leading to more dense structures wherein the release of trapped drug is postponed resulting in more sustained release. We further investigated how the initial thickness (height) of the ES, compared to the depth of the compartments in the cutting tool, would affect the final 3D structure and compactness of fibers in the MuNaMi. Due to the mass consistency between the original electrospun sheet (Fig. 9A) and the particles cut out of the electrospun sheet (Fig. 9B), comparing the corresponding volumes is used to calculate the compactness level. The volume of the original ES which is cut to form a single particle is calculated according to Eq. (1), where "b" is the length of the base part of the cutting compartment and H_{es} is the thickness or height of the original electrospun sheet. The length of the upper part of the frustum pyramid ("a") is calculated to 27 μm, using the data of the cutting tool as mentioned in the legend of Fig. 1 and according to Eq. (2). The volume of the particle is considered the same as the cutting tool compartment according to Eq. (3) which is calculated to $4.9 * 10^{-4}$ mm^3. Three different PLGA electrospun sheets with thicknesses of around 150, 80 and 60 μm were used as the substrate for micro-cutting (Fig. 9C.D). As shown in Fig. 9D, a sharp pyramidal frustum shape is obtained when cutting through the thick sheet of 150 μm, whilst cutting through the other two leads to lower compression, less compactness, and more smooth structures. For the case of using electrospun sheet with original thickness of H_{es} = 150 μm, the V_{es} is calculated to $2.5 * 10^{-3}$ mm^3, and therefore the compactness ratio is around 80 % according to Eq. (4). Likewise, the compactness of the other two electrospun sheets of PLGA with H_{es} of 80 and 60 μm (Fig. 9D) is calculated to 64 % and 51 % respectively. Therefore, starting with ES of different thicknesses compared with the cutting tool is a scalable possibility to form particles of different compactness and tunable release profile. Similarly, we observed that the cutting procedure using a cylindrical

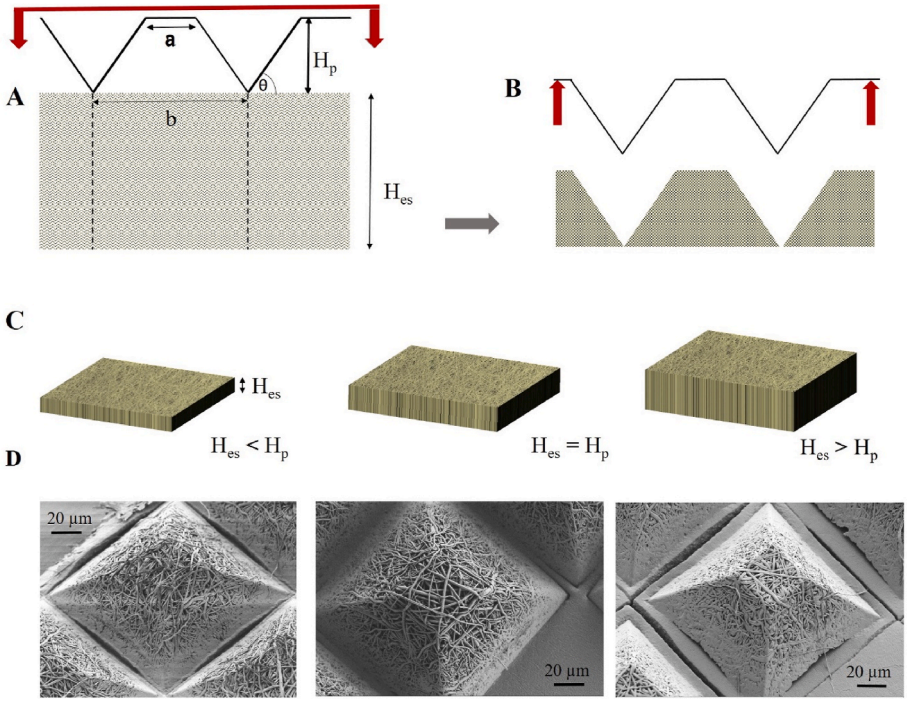

Fig. 9. Formulating MoNaMi constructs of different compactness and porosity depending on the original thickness of the ES (H_{es}) compared with the depth of cutting tool (H_p). Schematic demonstration of dimensional changes from an ES (A) to MoNaMi (B) and the relevance to the different original thicknesses of the ES (C), where final MoNaMi demonstrate increased compactness and sharpness of edges along with increasing the original thickness of sheets (D).

cutter on a monolayer ES leads to formation of highly dense structures in the area undergone cutting compared with the highly porous fibrous structure maintained in the adjacent area (Fig. 3S).

$$Volume\ of\ the\ ES\ making\ one\ particle: V_{es} = \left(H_{es} b^2\right) \tag{1}$$

$$Length\ of\ the\ square\ in\ the\ top\ part\ of\ the\ particle: a = b - 2\left(\frac{H_p}{tan\,\Theta}\right) \tag{2}$$

$$Volume\ of\ frustum\ pyramid\ particle: V_p = \frac{1}{3} H_p \left(a^2 + ab + b^2\right) \tag{3}$$

$$Compactness = \left(1 - \frac{V_p}{V_{es}}\right) \cdot 100 \tag{4}$$

4. Conclusion

Oral drug delivery is known as one of the most promising administration routes. Several studies have indicated advantages of nanostructured microfabricated systems for oral drug delivery. However, there are challenges that restrict these from becoming commercially available. In other words, several considerations such as 1) applying benign fabrication techniques avoiding destructive effects on the drugs such as organic solvents and local temperature increases, and 2) providing control over size, sustained delivery, and potential co-delivery of pharmaceutics should be taken into account. Our introduced micro-cutting technique meets all these demands thanks to the ultra-sharp custom-made cutting tools and the post transfer mechanical step to release the individual particles, where no heating or use of organic solvents is included as post-processing. Our MuNaMi constructs not only provide monodisperse particles (same size, shape and content), but also the possibility of sustained co-delivery of several components, bioactive agents or microorganisms loaded into different electrospun layers. The potential to tailor the level of compactness of the MuNaMi is a further advantage to optimize the release profile for drug delivery via other routes, or to apply these particles for dual cell-drug delivery where the nanofibrous structure of the particles serves as a platform for enhanced cell adhesion and proliferation besides the release of one or more active pharmaceutical ingredients.

Funding

This research was funded by the Novo Nordisk Foundation (NNF17OC0026910), MIMIO–Microstructures, microbiota and oral delivery and by the Danish National Research Foundation (DNRF122) and Villum Foundation (Grant No. 9301), Center for Intelligent Drug Delivery and Sensing Using Microcontainers and Nanomechanics (IDUN).

Data availability statement

All raw data not shown in the main text or supplementary figures is available upon request to the corresponding author.

CRediT authorship contribution statement

Fatemeh Ajalloueian: Conceptualization, Formal analysis, Investigation, Methodology, Supervision, Validation, Writing – original draft, Writing – review & editing. **Lasse Hojlund Eklund Thamdrup:** Conceptualization, Formal analysis, Investigation, Methodology, Validation, Writing – original draft, Writing – review & editing. **Chiara Mazzoni:** Formal analysis, Methodology, Validation, Writing – review & editing. **Ritika Singh Petersen:** Data curation, Validation, Writing – review & editing. **Stephan Sylvest Keller:** Data curation, Validation, Writing – review & editing. **Anja Boisen:** Conceptualization, Resources, Writing – review & editing.

Declaration of competing interest

The authors declare no competing interests. However, we would like to disclose that the Technical University of Denmark has filed a patent (PCT/EP2024/055263) entitled "Monodisperse nanofibrous microparticles for delivery of one or more active substances" where the inventors are Ajalloueian F., Thamdrup L.H.E. and Boisen A.

Appendix A. Supplementary data

Supplementary data to this article can be found online at https://doi.org/10.1016/j.heliyon.2024.e30844.

References

[1] R. Alany, Oral dosage forms and drug delivery systems: tablets, oral films, liquid dosage forms, oral bioavailability enhancement Raid Alany, Pharm Dev Technol 22 (2) (2017), https://doi.org/10.1080/10837450.2017.1281543, 137-137.

[2] B. Homayun, X. Lin, H.J. Choi, Challenges and recent progress in oral drug delivery systems for biopharmaceuticals, Pharmaceutics 11 (3) (2019), https://doi.org/10.3390/pharmaceutics11030129.

[3] A.A. Abdellatif, Microparticles Formulation as a Targeting Drug Delivery System, J Nanomed Res 6 (2017), https://doi.org/10.15406/jnmr.2017.06.00151.

[4] S. Murugesan, B. Gowramma, K. Lakshmanan, V.V.S. Reddy Karri, A. Radhakrishnan, Oral Modified drug release solid dosage form with special reference to design; an Overview, Curr Drug Res Rev 12 (1) (2019) 16–25, https://doi.org/10.2174/2589977511666191121094520.

[5] S.G. Carvalho, A. Martins, A.L. Polli, A.G. Tavares, Chorilli M, M.P. Daflon, Expert Opinion on Drug Delivery Multifunctional systems based on nano-in-microparticles as strategies for drug delivery : advances , challenges , and future perspectives, Expert Opin Drug Deliv 20 (9) (2023) 1231–1250, https://doi.org/10.1080/17425247.2023.2263360.

[6] S. Hua, Advances in oral drug delivery for Regional targeting in the gastrointestinal tract - influence of Physiological, Pathophysiological and pharmaceutical factors, Front. Pharmacol. 11 (2020), https://doi.org/10.3389/fphar.2020.00524.

[7] K. Elumalai, S. Srinivasan, A. Shanmugam, Biomedical Technology Review of the ef fi cacy of nanoparticle-based drug delivery systems for cancer treatment, Biomed Technol 5 (September 2023) (2024) 109–122, https://doi.org/10.1016/j.bmt.2023.09.001.

[8] H. Shahdadi Sardo, F. Saremnejad, S. Bagheri, A. Akhgari, H. Afrasiabi Garekani, F. Sadeghi, A review on 5-aminosalicylic acid colon-targeted oral drug delivery systems, Int J Pharm 558 (2019) 367–379, https://doi.org/10.1016/j.ijpharm.2019.01.022.

[9] Y. Zhao, Y. He, J. Guo, et al., Time-dependent bladder tissue regeneration using bilayer bladder acellular matrix graft-silk fibroin scaffolds in a rat bladder augmentation model, Acta Biomater. 23 (2015) 91–102, https://doi.org/10.1016/j.actbio.2015.05.032.

[10] P. Ma, X. Si, Q. Chen, et al., Oral drug delivery systems for ulcerative colitis therapy: a Comparative study with microparticles and nanoparticles, Curr. Cancer Drug Targets 19 (4) (2018) 304–311, https://doi.org/10.2174/1568009618666181016152042.

[11] Q. Chen, X. Si, L. Ma, et al., Oral delivery of curcumin: via porous polymeric nanoparticles for effective ulcerative colitis therapy, J. Mater. Chem. B 5 (29) (2017) 5881–5891, https://doi.org/10.1039/c7tb00328e.

[12] D.M. Moss, P. Curley, H. Kinvig, C. Hoskins, A. Owen, The biological challenges and pharmacological opportunities of orally administered nanomedicine delivery, Expert Rev Gastroenterol Hepatol 12 (3) (2018) 223–236, https://doi.org/10.1080/17474124.2018.1399794.

[13] J. Reinholz, K. Landfester, V. Mailänder, The challenges of oral drug delivery via nanocarriers, Drug Deliv. 25 (1) (2018) 1694–1705, https://doi.org/10.1080/10717544.2018.1501119.

[14] R. Augustine, D.L. Ashkenazi, R.S. Arzi, V. Zlobin, R. Shofti, A. Sosnik, Nanoparticle-in-microparticle oral drug delivery system of a clinically relevant darunavir/ritonavir antiretroviral combination, Acta Biomater. 74 (2018) 344–359, https://doi.org/10.1016/j.actbio.2018.04.045.

[15] H. Shahdadi Sardo, F. Saremnejad, S. Bagheri, A. Akhgari, H. Afrasiabi Garekani, F. Sadeghi, A review on 5-aminosalicylic acid colon-targeted oral drug delivery systems, Int J Pharm 558 (2019) 367–379, https://doi.org/10.1016/j.ijpharm.2019.01.022.

[16] C.Y. Wong, H. Al-Salami, C.R. Dass, Microparticles, microcapsules and microspheres: a review of recent developments and prospects for oral delivery of insulin, Int J Pharm 537 (1–2) (2018) 223–244, https://doi.org/10.1016/j.ijpharm.2017.12.036.

[17] M.N. Singh, K.S.Y. Hemant, M. Ram, H.G. Shivakumar, Microencapsulation: a promising technique for controlled drug delivery, Res Pharm Sci 5 (2) (2010) 65–77.

[18] L.M. Spindler, A. Feuerhake, S. Ladel, et al., Nano-in-Micro-Particles consisting of PLGA nanoparticles Embedded in chitosan microparticles via Spray-Drying enhances their uptake in the Olfactory Mucosa, Front. Pharmacol. 12 (2021) 2282, https://doi.org/10.3389/FPHAR.2021.732954/BIBTEX.

[19] M. Ruggeri, B. Vigani, C. Boselli, et al., Smart nano-in-microparticles to tackle bacterial infections in skin tissue engineering, Mater Today Bio 16 (August) (2022), https://doi.org/10.1016/j.mtbio.2022.100418.

[20] F. Ajalloueian, S. Asgari, P.R. Guerra, et al., Amoxicillin-loaded multilayer pullulan-based nanofibers maintain long-term antibacterial properties with tunable release profile for topical skin delivery applications, Int. J. Biol. Macromol. 215 (2022) 413–423, https://doi.org/10.1016/J.IJBIOMAC.2022.06.054.

[21] T.A. Jeckson, Y.P. Neo, S.P. Sisinthy, B. Gorain, Delivery of therapeutics from layer-by-layer electrospun nanofiber matrix for wound Healing: an Update, J Pharm Sci 110 (2) (2021) 635–653, https://doi.org/10.1016/j.xphs.2020.10.003.

[22] S.K. Boda, S. Chen, K. Chu, H.J. Kim, J. Xie, Electrospraying electrospun nanofiber segments into injectable microspheres for potential cell delivery, ACS Appl. Mater. Interfaces 10 (30) (2018) 25069–25079, https://doi.org/10.1021/acsami.8b06386.

[23] J.V. John, A. McCarthy, H. Wang, et al., Engineering Biomimetic nanofiber microspheres with tailored size, Predesigned structure, and desired composition via gas Bubble–Mediated Coaxial Electrospray, Small 16 (19) (2020), https://doi.org/10.1002/SMLL.201907393.

[24] S. Yan, L. Wang, H. Fan, et al., Biomimetic Natural silk nanofibrous microspheres for Multifunctional biomedical applications, ACS Nano 16 (9) (2022) 15115–15123, https://doi.org/10.1021/acsnano.2c06331.

[25] C.G. Park, M.J. Kim, M. Park, et al., Nanostructured mucoadhesive microparticles for enhanced preocular retention, Acta Biomater. 10 (1) (2014) 77–86, https://doi.org/10.1016/J.ACTBIO.2013.08.026.

[26] G.L. Pérez-González, L.J. Villarreal-Gómez, A. Serrano-Medina, E.J. Torres-Martínez, J.M. Cornejo-Bravo, Mucoadhesive electrospun nanofibers for drug delivery systems: applications of polymers and the parameters' roles, Int J Nanomedicine 14 (2019) 5271, https://doi.org/10.2147/IJN.S193328.

[27] A. Dodero, M. Alloisio, M. Castellano, S. Vicini, Multilayer Alginate-polycaprolactone electrospun membranes as skin wound Patches with drug delivery Abilities, ACS Appl. Mater. Interfaces 12 (28) (2020) 31162–31171, https://doi.org/10.1021/acsami.0c07352.

[28] M. Forouharshad, F. Ajalloueian, Tunable self-assembled stereocomplexed-polylactic acid nanoparticles as a drug carrier, Polym. Adv. Technol. 33 (1) (2022) 246–253, https://doi.org/10.1002/PAT.5510.

[29] S. Asgari, A. Pourjavadi, M. Setayeshmehr, A. Boisen, F. Ajalloueian, Encapsulation of drug-loaded Graphene oxide-based Nanocarrier into electrospun pullulan nanofibers for potential local Chemotherapy of Breast cancer, Macromol. Chem. Phys. 222 (15) (2021) 2100096, https://doi.org/10.1002/MACP.202100096.

[30] Q. Liu, H. Jia, W. Ouyang, Y. Mu, Z. Wu, Fabrication of Antimicrobial multilayered nanofibrous scaffolds-loaded drug via electrospinning for biomedical application, Front. Bioeng. Biotechnol. 9 (2021) 897, https://doi.org/10.3389/FBIOE.2021.755777/BIBTEX.

[31] M.B. Stie, J.R. Gätke, I.S. Chronakis, J. Jacobsen, H.M. Nielsen, Mucoadhesive electrospun nanofiber-based Hybrid system with controlled and Unidirectional release of Desmopressin, 2022;23, Int. J. Mol. Sci. 23 (3) (2022) 1458, https://doi.org/10.3390/IJMS23031458, 1458.

[32] F. Ajalloueian, P.R. Guerra, M.I. Bahl, et al., Multi-layer PLGA-pullulan-PLGA electrospun nanofibers for probiotic delivery, Food Hydrocoll 123 (2022) 107112, https://doi.org/10.1016/J.FOODHYD.2021.107112.

[33] S. Fahimirad, F. Ajalloueian, Naturally-derived electrospun wound dressings for target delivery of bio-active agents, Int J Pharm 566 (2019) 307–328, https://doi.org/10.1016/J.IJPHARM.2019.05.053.

[34] S. Asgari, A. Pourjavadi, T.R. Licht, A. Boisen, F. Ajalloueian, Polymeric carriers for enhanced delivery of probiotics, Adv. Drug Deliv. Rev. 161–162 (2020) 1–21, https://doi.org/10.1016/j.addr.2020.07.014.

[35] S Homaeigohar, AR Boccaccini, Antibacterial biohybrid nanofibers for wound dressings, Acta Biomater 107 (2020), https://doi.org/10.1016/j.actbio.2020.02.022.

[36] S.M. Kamath, K. Sridhar, D. Jaison, et al., Fabrication of tri-layered electrospun polycaprolactone mats with improved sustained drug release profile, Sci Reports 10 (1) (2020) 1–13, https://doi.org/10.1038/s41598-020-74885-1, 101. 2020.

[37] R.S. Petersen, S.S. Keller, A. Boisen, Hot punching of high-aspect-ratio 3D polymeric microstructures for drug delivery, Lab Chip 15 (12) (2015) 2576–2579, https://doi.org/10.1039/c5lc00372e.

[38] M. Terakawa, Femtosecond laser processing of biodegradable polymers, Appl. Sci. 8 (7) (2018) 1–13, https://doi.org/10.3390/app8071123.

[39] H woon Choi, J.K. Johnson, J. Nam, D.F. Farson, J. Lannutti, Structuring electrospun polycaprolactone nanofiber tissue scaffolds by femtosecond laser ablation, J. Laser Appl. 19 (4) (2007) 225–231, https://doi.org/10.2351/1.2795749.

[40] Y. Wu, A.Y. Vorobyev, R.L. Clark, C. Guo, Femtosecond laser machining of electrospun membranes, Appl. Surf. Sci. 257 (2010) 2432–2435, https://doi.org/10.1016/j.apsusc.2010.09.111.
[41] R.S. Petersen, A. Boisen, S.S. Keller, Micromechanical punching: a versatile method for non-spherical microparticle fabrication, Polymers 13 (1) (2021) 1–9, https://doi.org/10.3390/polym13010083.
[42] D. Poudel, S. Swilley-sanchez, O. Sean, J. Matson, T. Long, C. Fernandez-Fraguas, Novel electrospun pullulan fibers Incorporating Hydroxypropyl-β-cyclodextrin: morphology and relation with Rheological properties, Polymers 12 (2020) 2558.
[43] J.F. Christfort, A.J. Guillot, A. Melero, et al., Cubic microcontainers improve in situ colonic mucoadhesion and absorption of amoxicillin in rats, Pharmaceutics 12 (4) (2020) 1–16, https://doi.org/10.3390/pharmaceutics12040355.
[44] M. Götze, O. Krimig, T. Kürbitz, S. Henning, A. Heilmann, G. Hillrichs, Processing of polyamide electrospun nanofibers with picosecond Uv-laser irradiation, Phys. Procedia 83 (2016) 147–156, https://doi.org/10.1016/j.phpro.2016.08.028.
[45] J. Schmid, S. Schwarz, M. Fischer, et al., A laser-cutting-based manufacturing process for the generation of three-dimensional scaffolds for tissue engineering using Polycaprolactone/Hydroxyapatite composite polymer, J. Tissue Eng. 10 (2019) 2041731419859157, https://doi.org/10.1177/2041731419859157.
[46] D. Han, R. Serra, N. Gorelick, et al., Multi-layered core-sheath fiber membranes for controlled drug release in the local treatment of brain tumor, Sci. Rep. 9 (1) (2019), https://doi.org/10.1038/s41598-019-54283-y.
[47] M. Milosevic, D.B. Stojanovic, V. Simic, et al., Preparation and modeling of three-layered PCL/PLGA/PCL fibrous scaffolds for prolonged drug release, Sci. Rep. 10 (1) (2020), https://doi.org/10.1038/s41598-020-68117-9.
[48] B.D. Kevadiya, L. Zhang, R.N. Davé, Sustained release of poorly water-soluble drug from hydrophilic polymeric film sandwiched between hydrophobic layers, AAPS PharmSciTech 19 (6) (2018) 2572–2584, https://doi.org/10.1208/s12249-018-1089-x.
[49] I. Arshad, S. Ali, U. Amin, et al., Effect of hydrophilic and hydrophobic polymer on the release of ketoprofen and allopurinol from bilayer matrix transdermal patch, Adv. Polym. Technol. 37 (8) (2018) 3076–3083, https://doi.org/10.1002/adv.22078.
[50] S. Tohidi, A. Ghaee, J. Barzin, Preparation and characterization of poly(lactic-co-glycolic acid)/chitosan electrospun membrane containing amoxicillin-loaded halloysite nanoclay, Polym. Adv. Technol. 27 (8) (2016) 1020–1028, https://doi.org/10.1002/pat.3764.
[51] C. Bisson-Boutelliez, S. Fontanay, C. Finance, F. Kedzierewicz, Preparation and physicochemical characterization of amoxicillin β-cyclodextrin complexes, AAPS PharmSciTech 11 (2) (2010) 574–581, https://doi.org/10.1208/s12249-010-9412-1.
[52] A Bebu, L Szabó, N Leopold, C Berindean, L. IR David, Raman, SERS and DFT study of amoxicillin, J. Mol. Struct. 993 (2011), https://doi.org/10.1016/j.molstruc.2010.11.067.
[53] J. Siepmann, F. Siepmann, Modeling of diffusion controlled drug delivery, J Control Release 161 (2) (2012) 351–362, https://doi.org/10.1016/j.jconrel.2011.10.006.